Southern Ocean Climate and Sea Ice Anomalies Associated with the Southern Oscillation

R. Kwok and J. C. Comiso*

Jet Propulsion Laboratory
California Institute of Technology
4800 Oak Grove Dr
Pasadena, CA 91109

**Laboratory for Hydrospheric Processes, Code 971*
NASA Goddard Space Flight Center
Greenbelt, MD

Abstract

The anomalies in the climate and sea ice cover of the Southern Ocean and their relationships with the Southern Oscillation (SO) are investigated using a 17-year of data set from 1982 through 1998. We correlate the polar climate anomalies with the Southern Oscillation index (SOI) and examine the composites of these anomalies under the positive (SOI > 0), neutral (0 > SOI > -1), and negative (SOI < -1) phases of SOI. The climate data set consists of sea-level pressure, wind, surface air temperature, and sea surface temperature fields, while the sea ice data set describes its extent, concentration, motion, and surface temperature. The analysis depicts, for the first time, the spatial variability in the relationship of the above variables and the SOI. The strongest correlation between the SOI and the polar climate anomalies are found in the Bellingshausen, Amundsen and Ross sea sectors. The composite fields reveal anomalies that are organized in distinct large-scale spatial patterns with opposing polarities at the two extremes of SOI, and suggest oscillating climate anomalies that are closely linked to the SO. Within these sectors, positive (negative) phases of the SOI are generally associated with lower (higher) sea-level pressure, cooler (warmer) surface air temperature, and cooler (warmer) sea surface temperature in these sectors. Associations between these climate anomalies and the behavior of the Antarctic sea ice cover are clearly evident. Recent anomalies in the sea ice cover that are apparently associated with the SOI include: the record decrease in the sea ice extent in the Bellingshausen Sea from mid-1988 through early 1991; the relationship between Ross Sea SST and ENSO signal, and reduced sea ice concentration in the Ross Sea; and, the shortening of the ice season in the eastern Ross Sea, Amundsen Sea, far western Weddell Sea, and the lengthening of the ice season in the western Ross Sea, Bellinghausen Sea and central Weddell Sea gyre over the period 1988-1994. Four ENSO episodes over the last 17 years contributed to a negative mean in the SOI (-0.5). In each of these episodes, significant retreats in the Bellingshausen/Amundsen Sea were observed providing direct confirmation of the impact of SO on the Antarctic sea ice cover.

To be submitted to the Journal of Climate

Southern Ocean Climate and Sea Ice Anomalies Associated with the Southern Oscillation

R. Kwok and J. C. Comiso*

Jet Propulsion Laboratory
California Institute of Technology
4800 Oak Grove Dr
Pasadena, CA 91109

**Laboratory for Hydrospheric Processes, Code 971*
NASA Goddard Space Flight Center
Greenbelt, MD

To be submitted to J. Climate

Southern Ocean Climate and Sea Ice Anomalies Associated with the Southern Oscillation

R. Kwok and J. C. Comiso

Abstract

The anomalies in the climate and sea ice cover of the Southern Ocean and their relationships with the Southern Oscillation (SO) are investigated using a 17-year of data set from 1982 through 1998. We correlate the polar climate anomalies with the Southern Oscillation index (SOI) and examine the composites of these anomalies under the positive (SOI > 0), neutral (0 > SOI > -1), and negative (SOI < -1) phases of SOI. The climate data set consists of sea-level pressure, wind, surface air temperature, and sea surface temperature fields, while the sea ice data set describes its extent, concentration, motion, and surface temperature. The analysis depicts, for the first time, the spatial variability in the relationship of the above variables and the SOI. The strongest correlation between the SOI and the polar climate anomalies are found in the Bellingshausen, Amundsen and Ross sea sectors. The composite fields reveal anomalies that are organized in distinct large-scale spatial patterns with opposing polarities at the two extremes of SOI, and suggest oscillating climate anomalies that are closely linked to the SO. Within these sectors, positive (negative) phases of the SOI are generally associated with lower (higher) sea-level pressure, cooler (warmer) surface air temperature, and cooler (warmer) sea surface temperature in these sectors. Associations between these climate anomalies and the behavior of the Antarctic sea ice cover are clearly evident. Recent anomalies in the sea ice cover that are apparently associated with the SOI include: the record decrease in the sea ice extent in the Bellingshausen Sea from mid-1988 through early 1991; the relationship between Ross Sea SST and ENSO signal, and reduced sea ice concentration in the Ross Sea; and, the shortening of the ice season in the eastern Ross Sea, Amundsen Sea, far western Weddell Sea, and the lengthening of the ice season in the western Ross Sea, Bellinghausen Sea and central Weddell Sea gyre over the period 1988-1994. Four ENSO episodes over the last 17 years contributed to a negative mean in the SOI (-0.5). In each of these episodes, significant retreats in the

Bellingshausen/Amundsen Sea were observed providing direct confirmation of the impact of SO on the Antarctic sea ice cover.

1. Introduction

The Southern Oscillation (SO) refers to the seesaw in the surface pressure anomalies between the Indian Ocean-Australian region and the southeastern tropical Pacific on a seasonal and interannual time scale. The large scale character of the SO in the tropics and subtropics in the Southern Hemisphere is well-known [*Philander and Rasmusson*, 1985]. The SO has a signature that extends to the mid- and high-latitudes in the Southern Hemisphere in the winter and summer. The high latitude signature of the SO have associated anomalies over the Antarctic ice cover. Understanding these links between the SO and Antarctic sea ice cover are important due to the high sensitivity of sea ice to anomalies in climate forcing. Sea ice interacts with the global climate over a broad range of spatial and temporal scales [*Schlesinger and Mitchell*, 1985; *Manabe et al.*, 1991]. Sea ice albedo feedback involves changes in the climatological area of the ice cover and adjustments in the poleward heat transport by the atmosphere, in addition to changes in the thickness, albedo, and temperature of ice within the Antarctic ice pack. The ocean structure and circulation are affected during sea ice growth, as salt is rejected to the underlying ocean, increasing its density, and leading sometimes to deep ocean convection and bottom water formation. Equatorward transport of ice results in a net flux of freshwater and negative heat. Thus, anomalies in these polar processes have complex consequences in the global climate.

Many studies have analyzed the recent behavior of the Antarctic ice extent [*Jacobs and Comiso*, 1993; *Jacobs and Comiso*, 1997] and have suggested connections between the ice extent and the Southern Oscillation [*Carleton*, 1988; *Simmonds and Jacka*, 1995; *Gloersen, 1995*; *Ledley and Huang*, 1997; *Gloersen and Mernicky, 1998*]. Using a 12-year data set (1985-1994), *White and Petersen* [1996] found coupled anomalies that propagate eastward with the Antarctic Circumpolar Current (ACC) with a period of 4-5 years (wavenumber-2) and taking 8-10 years to encircle Antarctica. It was suggested that this Antarctic Circumpolar Wave (ACW) is associated with ENSO related activities in the equatorial Pacific, possibly through an atmospheric teleconnection with higher

southern latitudes. *Peterson and White* [1998], in a case study, show ENSO can be a possible source of the interannual anomalies for sustaining the ACW in the western subtropical South Pacific. *Parkinson* [1998] also suggests that the lengthening/shortening sea ice season might be related to the variability of the ACW. *Bonekamp et al.* [1999] in an examination of the European Center for Medium Range Weather Forecast Atmospheric Reanalysis (ERA) data set from 1979 through 1994, however, did not find eastward propagating anomalies suggestive of an ACW prior to 1984. For that time period at least, a two-regime structure with and without the presence of ACW was indicated. In a recent study, *Yuan and Martinson* [2000] explored possible relationships between the record of Antarctic sea ice extent between 1978-1996 and global climate variability. They found a strong link of the sea ice edge anomalies in the Amundsen, Bellingshausen, and Weddell Seas to extrapolar climate.

The objective of this project is to study in good spatial detail, the teleconnections between SO and the anomalies in the Southern Ocean climate including its sea ice cover. Our approach is to analyze the linear correlation of the Southern Oscillation index (SOI) with the polar climate anomalies, and to examine the composites of these anomalies during three phases of the SOI which we define as: SOI > 0, 0 > SOI > -1, and SOI < -1, and refer to as the positive, neutral, and negative phases. The data sets used here span a 17-year period from 1982 to 1998. Our study takes advantage of new data on ice motion and ice surface temperature derived from passive microwave imagery and NOAA/AVHRR (A Very High Resolution Radiometer) data. Rather than having to restrict our study area to the ice edge region, as was done previously [*White and Peterson*, 1996], this data set allows a more detailed examination of the spatial signatures of the climate and sea ice anomalies.

The paper is organized as follows. In Section 2, we describe the climate and sea ice data sets used in our analysis. Section 3 presents the spatial pattern of correlation between the Southern Ocean climate anomalies and the SOI, and the composite patterns of the climate and sea ice anomalies associated with three phases of the SOI over the 17 years. We

discuss our results in the context of previous work in Section 4. The paper is summarized in the last section.

2. Data Description

2.1 Climate Data

The monthly Southern Oscillation Index (SOI) used in this study were those of the Climate Analysis Center. The SOI is the difference between the standardized Tahiti sea-level pressure (SLP) and the standardized Darwin SLP measurements. Large negative excursions of the SOI are associated with intense El Niño-Southern Oscillation (ENSO) episodes (Fig. 1). Between 1982 and 1998, there were four ENSO episodes in 1983, 1987, 1992, and 1998 occurring at approximately the same frequency and with approximately the same duration. This can be seen in the strong 4-yr peak and 2.5-yr secondary peak in the spectral amplitude of the SOI time series over the 17-years between 1982 and 1998. In the analyses that follow, we use a 3-month running average of the SOI to avoid a significant portion of the noise due to small-scale and transient phenomena that are not associated with the large scale coherent SO signal [*Trenberth*, 1984].

Monthly sea-level pressure (SLP), zonal and meridional winds (ZW, MW), and surface air temperature (SAT) anomalies are computed from the National Centers for Environmental Prediction (NCEP) – National Center for Atmospheric Research (NCAR) reanalysis output [*Kalnay et al.*, 1996]. The anomaly fields in the global NCEP 2.5° by 2.5° grid are resampled onto a polar stereographic grid for better visualization of the anomalies over the circumpolar Southern Ocean. Likewise, monthly sea surface temperature (SST) anomalies are resampled onto this same format. The mean monthly SST data on a 1° grid are the optimally interpolated fields of *Reynolds and Smith* [1994]. Monthly anomalies are produced by first creating the monthly means, removing the monthly climatology. and then de-trending the time series at each sample.

2.2 Sea Ice Data

The 17 years of sea ice extent (SIE) and gridded sea ice concentration (SIC) derived from satellite passive microwave data are provided by the National Snow and Ice Data Center (NSIDC). Due to the dissimilarity of the SMMR and SSM/I sensors and mapping strategies, analyzed daily fields of SIE and SIC are available only after 1988. Prior to 1988, only 2-day SIE and SIC fields are available. We define the sea ice extent as the mean latitudinal location of the ice edge over 10^{o} sectors around the Antarctic continent.

Optimally interpolated fields of sea ice motion (SIM) [*Kwok et al.*, 1998] are provided by the JPL Remote Sensing Group. These analyzed motion fields are created by blending ice motion derived from two channels of satellite passive microwave data (37 GHz and 85 GHz) and available ice displacements from drifting buoys. Only ice motion fields between March and November are available since ice tracking results are unreliable during the summer and seasonal transitions. The monthly meridional (MIM) and zonal ice motion (ZIM) are on a 100-km polar stereographic grid.

The January and July mean sea ice surface temperature (IST) data used in this study were derived from AVHRR infrared data. Because of persistent cloudiness in the Antarctic region and the difficulty of discriminating clouds from snow covered ice, a special cloud masking procedure was utilized, in addition to conventional techniques used over open ocean. Details of the retrieval procedure can be found in *Comiso* [2000]. The uncertainty in the retrievals is estimated to be generally less than 3^{o}K over ice-covered surfaces and less than 1^{o}K over open ocean. The data are mapped onto the polar stereographic format used for SSM/I data, with a grid size of 6.25 km.

Similar to the climate data set, all monthly sea ice anomalies are produced by first creating the monthly means, removing the monthly climatology and then de-trending the time series at each sample location.

3. Data Analysis

3.1 Correlation and Composites Fields

In this section, we examine the polar climate and sea ice anomalies associated with the SOI by correlation of the SOI time-series with the climate anomalies and by forming composites of the climate and sea ice anomalies under the three phases of SOI defined above. At each sample location, the correlation coefficients between the time-series of SLP, MW, ZW, SAT, and SST anomalies and the SOI time series are computed. The resulting correlation fields are shown in Fig. 2. The statistical significance of the normalized cross-correlation coefficients depends on the length of the data set and the smoothing applied. In the 17-year data set, there are 204 monthly data points or 202 degrees of freedom. Thus, the correlation coefficients are statistically significant at the 95% level if they exceed ~0.14 [*Bendat and Piersol*, 2000]. With the 3-point smoothed SOI time-series, the number of degrees of freedom reduces to ~67 after accounting for the effect of auto-correlation. In this case, the correlation coefficients are statistically significant at the 95% level if they exceed a threshold of ~0.25.

Composite fields from three different phases of the SOI (SOI > 0, 0 > SOI > -1, SOI < -1) are constructed by averaging the monthly anomaly fields that fall within each of the three ranges of the SOI index. Note that the phases that we select are not symmetric about zero. The rationale for this division is that over the 17 years between 1982 and 1998, the mean of the SOI index is non-zero and has a significant bias of -0.5. The division into these ranges gives us an approximately equal number of anomaly fields in each composite. The number of anomaly fields contained in each of the three phases positive (SOI^+), neutral (SOI^0), and negative (SOI^-) phases are 53, 72, and 53. These composites allow us to examine the dominant spatial pattern of the anomalies associated the oscillatory behavior of the SOI. In the remainder of this section, we describe the patterns observed in the correlation maps and the composite fields, and comment on the stability of the anomaly fields.

3.2 Polar Climate Anomalies

The correlation amplitudes show distinct centers of action in the correlation maps (positive and negative extremes in the correlation coefficient) of the polar climate anomalies and SOI (Fig. 2). The lag-correlation plots between the time-series of climate anomalies and SOI at the locations of strongest positive and negative correlation south of 50°S are shown in Fig. 3. We examine only the peaks in the higher latitudes because the signals in the tropical and mid-latitudes are dominated by the SO pattern. Fig. 4 shows the composite fields of climate anomalies under the three phases (SOI^+, SOI^0, SOI^-) of SOI as well as the difference between the SOI^+ and SOI^- composites. This difference field is useful in accentuating the contrast between the two extreme phases.

Sea level pressure/winds

Over the entire domain, the SLP-SOI correlation map is dominated by the region of strong negative correlation (Fig. 2) in the eastern Indian Ocean northwest of Australia and the region of strong positive correlation in the subtropical eastern Pacific near Tahiti. This is the expected SLP anomaly pattern associated with the Southern Oscillation. Poleward of 50°S, there are three centers of action in the following regions: a sector of negative correlation between the Ross sea and the Antarctic Peninsula (peak ~ -0.42) flanked by two narrower sectors of weaker positive correlation east of the Weddell Sea and west of the Ross Sea. Negative correlation indicates a time-series of SLP anomalies that is out-of-phase with the SOI. In an analysis of the teleconnections in the Southern Hemisphere, *Mo and White* [1985] also found that zonally averaged pressure anomalies at sea level display an out-of-phase relation between low and high latitudes, and in mid-latitudes are negatively correlated with anomalies in the subtropics and polar regions. They suggested a strong resemblance to the oscillatory behavior associated with the SO as is seen here.

Between 50°S and 60°S, the SLP-SOI correlation field exhibits a wavenumber-2 pattern around the circumpolar Southern Ocean. As seen in the lag-correlation plots (Fig. 3) the spatial peaks are also distinct in time and the broad correlation structure shows similarity to the autocorrelation signature of the large-scale coherent SOI signal (Fig. 3). There is

no observable lag between the SLP anomalies and SOI at the location of the negative peak (centered between the Amundsen and Bellingshausen Seas). An ~2-month lag, with the SLP anomalies lagging the SOI, is evident at the location of the positive peak (centered along the prime meridian).

In the SOI^- SLP composite (Fig. 4), the typical ENSO pattern of positive SLP anomalies over northwest Australia and negative SLP anomalies over the subtropical eastern Pacific can be seen. The SO, indicated by large negative SOI indices, has a signature that clearly extends to the mid- and polar-latitudes of the Southern Hemisphere. South of 50°S, two distinct spatial patterns of SLP are associated with the two extreme phases of SOI. In the SOI^+ SLP composite, a sector of negative SLP anomaly is located off the Antarctic coast in the Amundsen and Bellingshausen Seas. An almost exact anomaly pattern of opposite polarity can be found in the SOI^- SLP composite.

This above normal SLP south of 50°S associated with ENSO episodes (SOI^-) was reported by *Karoly* [1989] but the strength of the pattern and the opposite behavior during SOI^+ are shown for the first time with some spatial detail in this study. It is interesting to note that the SLP anomalies in the sector between 170°W and 60°W is more spatially localized and more extreme than SLP anomalies at the two centers of action of the SO in the tropical latitudes. Within the domain shown in Fig. 4, the highest SLP anomaly can be found in the middle of the Amundsen and Bellingshausen Seas. The strong correlation of the region with ENSO episodes indicates that the climate anomalies in the region [*Jacobs and Comiso*, 1997; *King and Harangozo*, 1998], are associated with occurrences of ENSO. Between the two extremes (SOI^0), the anomalies are smaller. These composite patterns are persistent but varying in intensity throughout the year as observed in the December/January/February (DJF), March/April/May (MAM), June/July/August (JJA), and September/October/November (SON) composites (not shown here). The most extreme pattern can be seen in the SON fields.

The SLP anomalies alter the meridional and zonal wind anomalies which in turn affect the SIM and SIE. Wind anomalies cause changes in the transport of sea ice and air

masses, and changes in the freezing rate. The SOI-MW correlation field (Fig. 2) shows a sector of positive correlation between the Ross Sea (170°E) and east Amundsen Sea (100°W) and a sector of negative correlation between the Bellingshausen Sea and the Antarctic Peninsula. The ZW-SOI correlation map shows a sector of positive correlation between 50°S and 60°S between the Ross Sea and north of the Antarctic Peninsula. A narrow band of negative correlation, within the sea ice cover, can be found south of 60°S along the Antarctic coast in the Amundsen and Bellingshausen sectors. These patterns are consistent with the anomalous circulation patterns due to the SLP anomalies discussed above.

Similar to the SLP composites, the MW and ZW anomalies have distinct spatial patterns and opposite polarities at the SOI extremes (Fig. 4). Here, a sector of positive MW anomalies covering the Ross Sea and the Amundsen Sea can be found in the SOI+ composite. The negative MW anomalies straddles the Antarctic Peninsula and covers a sector containing part of the Bellingshausen Sea and Weddell Sea. Opposite patterns are found during SOI⁻. South of 60°S in the SOI⁻ ZW composites, positive zonal wind anomalies can be found in the Amundsen and Bellinghauen Seas, and parts of the Weddell Sea. North of 60°S, there is a large sector with negative ZW anomalies.

Surface air temperature

Three distinct SOI-SAT correlation bands can be seen in the Pacific Ocean sector (Fig. 2). A band of negative correlation in the equatorial Pacific, a band of positive correlation between 30°S and 45°S, and a band of negative correlation south of 50°S. Negative correlation indicates warmer SATs associated with negative excursions of the SOI. South of 50°S, there are two centers of action: a sector of negative correlation (negative peak~ -0.59) centered between the Ross Sea and the western Bellingshausen Sea and a sector of positive correlation (peak ~ 0.44) centered between the Bellingshausen Sea and the Weddell Sea. Both the positive and negative peaks lag the SOI by ~2-3 months.

The three bands in the SOI⁻ SAT composites (Fig. 4) are associated with warm/cold/warm anomalies in the tropical and sub-tropical Pacific during ENSO

episodes. Similarly, the SOI^+ and SOI^- SAT composites present two distinct and opposite patterns of SAT anomalies. South of 50°S, the SOI^+ SAT composite shows a sector of below normal SAT in the region between the Ross Sea and the Amundsen Sea and a sector of warmer SAT covering the Bellingshausen Sea and Weddell Sea. Again, an approximate opposite pattern is seen during SOI^-. These patterns are robust in the seasonal fields, with the SON field showing the largest extremes. A pronounced wavenumber-2 pattern encircling the pole is evident.

Sea surface temperature

The SAT and SST correlation maps (Fig. 2) are similar, three correlation bands can be seen in the Pacific Ocean: negative correlation covers one band in the equatorial Pacific, a mid-latitude band of positive correlation between 30°S and 45°S, and a band south of 50°S. Warmer SSTs are associated with negative excursions of the SOI. South of 50°S and off the sea ice zone, there are two centers of action: a sector of strong negative correlation (peak ~ -0.7) centered between the Ross and western Bellingshausen Seas and a sector of positive correlation (peak ~ 0.5) south of Tasmania. Distinct peaks can be seen in the lag-correlation plots. The negative correlation peak lags the SOI by 2-3 months.

Similar to the SAT, three bands in the SOI^- SST composites are associated with warm/ cold/warm sea surface temperature anomalies in the Pacific during ENSO episodes. South of 50°S, two distinct and opposite patterns of SST anomalies are associated in the SOI^+ and SOI^-. A sector of above SST can be seen in the region between the Ross and western Bellingshausen Seas in the SOI^- SST composite. This is associated with the large positive SST anomalies in the central equatorial Pacific Ocean. The approximate opposite pattern is seen during SOI^+. A wavenumber-2 pattern is seen in both the correlation and composite fields.

Summary of Polar Climate Anomalies

As revealed in the correlation maps and anomaly composites, the co-varying climate anomalies in the Amundsen, Bellingshausen, and Weddell Seas show the strongest link to the SOI. The spatial structure of the connections between the anomalies and SOI are

localized and well-defined. Within these sectors, positive (negative) phases of the SOI are generally associated with lower (higher) sea-level pressure, cooler (warmer) surface air temperature, and cooler (warmer) sea surface temperature in these sectors. The SLP, SAT, and SST correlation fields and composites show wavenumber-2 patterns that suggest of the anomalies at 56°S reported in *White and Petersen* [1996] although the peaks in these anomalies are found south of 60°S. The composite fields depict the mean anomalies over the three ranges of SOI defined here. In all the composites, it is remarkable that the anomaly patterns associated with the two extremes are distinct and are of opposite polarities. The broad correlation structure seen in the lag-correlation plots shows similarity to the autocorrelation signature of the large-scale coherent SOI signal (Fig. 3). The lag-correlations at the correlation peaks are interesting in that in all cases the SOI is either contemporaneous or leads the SLP, SAT, and SST fields. The underlying mechanisms are, however, not well-understood.

3.3 Antarctic Sea Ice Anomalies

Sea ice motion

The three composites of ice motion are shown in Fig. 5. Through wind forcing, the SLP anomalies over the Antarctic ice cover are coupled to the anomaly patterns of sea ice circulation. Anomalies in ice motion affect ice transport and ice extent. The pattern of winter (March through November) meridional (MIM) and zonal (ZIM) ice motion anomalies are well-correlated with the MW and ZW anomalies. This is not unexpected since away from coastal boundaries, geostrophic wind explains more than 70% of the variance of daily ice motion in both winter and summer. During SOI^+, a broad sector of positive MIM anomalies covers the Ross and Amundsen Sea ice covers. The negative MIM anomalies are located in the Bellingshausen and Weddell Seas. The SOI^- MIM composite shows anomalies of the opposite polarity compared to the SOI^+ MIM composite. In the SOI^0 composite, a sector of positive anomaly can be found covering the ice cover between 20°W and 20°E.

Similarly, ZIM anomalies are coupled to the ZW anomalies. Negative (positive) ZIM anomalies in the SOI^+ (SOI^-) composites cover the Amundsen and Bellinghausen Seas.

Under SOI^- conditions, a sector of positive ZIM anomalies can be found east of the Weddell Sea centered around the prime meridian. Extremes in ZIM anomalies can be found during the austral winter over the months of JJA and SON (not shown here).

Ice surface temperature

Fig. 6 shows the composites of IST/SST anomalies, derived from AVHRR data, for January (top panel) and July (lower panel). The anomaly patterns, especially those for July, resemble those of the SAT patterns discussed previously. A distinct wavenumber-3 pattern can be seen in the July SOI composites. Alternating positive and negative IST anomalies can be seen to cover three zones of the ice cover during SOI^+ with positive anomalies covering: the Amundsen and Weddell Seas; between 50°E and 100 °E; and, between 120 °E and 170°W. Opposite anomalies are observed during SOI^-. The significance of IST anomalies over the ice cover is that they affect the radiation balance at the surface and thus the rate of ice growth and brine rejection into the ocean.

These IST anomalies are also associated and resembles those of the SST near the ice edge. This is especially evident with the negative (positive) SST anomalies in the Amundsen and Ross Seas during SOI^+ (SOI^-).

Sea ice extent/sea ice concentration

The composites of SIE and SIC anomalies associated with the three phases of SOI are shown in Fig. 7. In the SOI^+ (SOI^-) composites, positive (negative) anomalies of the SIE are located between 180°W and 130°W in the Ross and Amundsen Seas, negative (positive) anomalies can be found between 100°W and 10°E in Bellingshausen and Weddell Seas, and, smaller positive (negative) anomalies are found in the sector between 10°E and 50°E. The anomalies in the other sectors of the Antarctic are insignificant during all three phases of the SOI. It is interesting to note that the SIE anomalies in the eastern Bellingshausen Sea are out-of-phase with those in the Amundsen Sea even though they are geographically contiguous. This out-of-phase relationship between the Bellingshausen and Amundsen sea ice edge can also be seen in the circumpolar lag-

correlation between the SOI and SIE anomalies (Fig. 8). The SOI lags the SIE anomalies in the Bellingshausen and eastern Weddell Seas by 2-3 months while the SOI leads the SIE in the Amundsen and Ross Seas. At zero lag, a wavenumber-2 pattern is also evident in the plot. The diagonal bands in Fig. 8 hint of eastward propagating SIE anomalies (associated with the SOI) between 180°E and 360°E with a circumpolar period of ~7-8 years (ACW-like signal) but this propagating pattern is not evident over the East Antarctica sea ice cover.

The largest SIC anomalies are located off the Antarctic coast near the ice edge. Also, the SIC anomalies are co-located within the same sectors as those of the SIE anomalies. Figs. 7 and 8 show that positive anomalies of the SIE are coupled with positive SIC anomalies while negative SIE anomalies are associated with negative SIC anomalies. This association of SIE and SIC anomalies of the same polarity would seem counter-intuitive if SIE anomalies are explained only by wind and ice motion, as divergence (convergence) would lead to negative (positive) ice concentration anomalies. The positive (negative) anomalies in the ice edge especially in the Ross and Amundsen Seas are indeed associated with positive (negative) anomalies in the meridional winds and ice motion (Fig. 4). However, these are also associated with negative (positive) anomalies in the SST and IST (Figs. 4 and 6) that favor (discourage) ice growth. As a result, the positive (negative) MW anomalies and ice motion anomalies favors expansion (retreat) in the ice edge, while cooler (warmer) SST and IST also allow ice growth (melt) in place and thus the relative persistence of the ice cover or higher (lower) ice concentration. This suggests that the ice edge and ice concentration anomalies are sustained by ice kinematics as well as thermodynamics with significant roles played by the anomalies in the SST and SAT.

The region with the most significant connection with the Southern Oscillation in the Southern Ocean is the Bellingshausen/Amundsen/Ross Sea region. Spatially distinct anomaly patterns in the climate as well as sea ice variables are apparent in the vicinity of this region. The teleconnection is clearly indicated in the plots of monthly time series of sea ice extent and ice area anomalies as shown in Figure 9. In both ice extent and ice area plots, anomalously low values occurred in 1983, 1987, 1992, and 1998. These are

the same years that were pointed out earlier (see Fig. 1) as ENSO years. It is interesting to note that similar anomalies for the same years did not occur in the sea ice variables in other Antarctic regions. The satellite time series in fact shows that the climatological behavior of the ice cover in the Bellingshausen/Amundsen Sea region is unique in its relation to the Southern Oscillation. This is the only region with an observable negative trend in ice cover over the last 20 years. A question of interest is whether the climate of the region is different from other regions because of the connection to the Southern Oscillation.

3.4 Stability of Composite Fields

The composite fields described in the previous section have been prepared over a relatively short 17-year period. An assessment of the stability of these composites has been carried out in two ways. First, the climate data are divided up into two eight-year records to determine whether the anomalies are spatially stable and give comparable magnitude of anomalies in the same regions. In all cases, the differences are minor and do not change the conclusions drawn here. Second, we produced seasonal composites (DJF, MAM, JJA, SON) to examine the stability of the anomalies constructed in this manner. While the locations of the anomalies remain relatively stable in the seasonal fields, the magnitudes do vary. The seasonal dependence of the magnitude of the anomalies, even though not shown here, is discussed in the text in the previous section.

4. Discussion

In this section, we discuss in more detail the co-varying climate and sea ice anomalies in the context of the results from previous studies. Clearly, the correlation maps and the anomaly composites show coherent links between the Southern Ocean climate and sea ice processes and the Southern Oscillation. The question is whether our results describing the associations between the SOI and sea ice anomalies are consistent with observations of sea ice anomalies from previous studies.

Sea ice cover and SOI

A number of studies have focused on the record of the Southern Ocean sea ice extent/edge and its relationship to climate variables and indices. Here, these observed trends and anomalies are discussed within the context of our results that describe the large-scale sea ice anomalies associated with the three phases of SOI over the 17-year period between 1982-1998.

Jacobs and Comiso [1993] attributed the record decrease in the sea ice extent in the Bellingshausen Sea from mid-1988 through early 1991 to more southerly surface winds and historic high surface air temperatures along the west coast of the Antarctic Peninsula in 1989. They also reported that this retreat was preceded by a higher than normal ice cover in 1986-87. An updated plot (1978-1999) of the monthly ice extent and ice area anomalies in the Bellingshausen/Amundsen Sea sector is shown in Fig. 9. Our composites (in Fig. 2 through 7) show a large-scale view of the associated climate and sea ice anomalies that are consistent with their observations. The period between 1986 through early 1991 brackets a period with an ENSO episode (SOI^-) in 1987 followed by a La Niña event (SOI^+) in 1989. Over this period, a positive anomaly followed by a negative anomaly in the Bellingshausen Sea ice cover are clearly seen in the SOI^- (SOI^+) SIE anomaly composites. The positive (negative) anomaly in ice extent is associated with cooler (warmer) SATs and ISTs, and positive (negative) meridional winds and ice motion anomalies due to the positive (negative) SLP anomalies in the Amundsen and Bellingshausen Seas. Thus, an above normal ice cover during SOI^- is followed by a below normal ice cover during SOI^+. This contrast in the ice extent over the two phases of SO accentuates the observed retreat of the ice cover.

In another study using an ice extent data set spanning 1973 and 1994, *Jacobs and Comiso* [1997] reported a decline in the sea ice extent of the Amundsen and Bellingshausen Seas in two decades following 1973. The northern ice edge retreated by ~1° of latitude in all seasons from 1973-79 to 1987-93 (also see Fig. 9). They suggest that the mean and extreme ice extents are linked to large-scale circulation changes in the South Pacific. Over the 21-year period from 1973-93, the linear trend of the SOI shows a significant decrease of -1.6 (standard deviation = 1.2) from 0.4 to -1.2. In the progression from SOI^+

to SOI conditions over the period, our composites (Figs. 2-7) show increasing SSTs, SATs, ISTs, and more northerly wind conditions in a large part of the Amundsen and western Bellingshausen Seas. The trend is also toward negative SIE anomalies in the Amundsen Sea. The positive SIE anomalies in the Bellingshausen Sea was not mentioned in the study since the SIE of the two seas were not treated separately, and the Amundsen Sea ice cover dominates the pattern. Again, our composite fields can be used to explain the general conditions of the ice cover associated with the Southern Oscillation.

Simmonds and Jacka [1995] explored links between Antarctic sea ice extent and the SOI using a data set spanning 1973-1992. They found correlations in the southwest Indian Ocean sector, the southwest and southeast Pacific Ocean sector, and a sector to the west of the Ross Sea. Their exploratory procedure was to calculate the correlation of the sea ice extent, averaged over various longitudinal domains in each calendar month, with the smoothed SOI values in all months in the same year and also the previous year and subsequent years. Their approach has the advantage of being able to localize the seasonal correlations with SOI, but their results are limited by a rather short data span of 20 points (or 18 degrees of freedom). Here, we compute the correlations based on the entire time series of SOI and ice edge anomaly. In this case the results are slightly different, they did not report the significant correlations in the Amundsen Sea, Bellingshausen Sea, and Weddell Gyre found here and are also reported by *Yuan and Martinson* [2000].

Ledley and Huang [1997] and *Gloersen* [1995]examined the sea ice concentration between 1982-1994 (which covered three ENSO episodes) and found that there is a statistically significant relationship between Ross Sea SST and sea ice concentration, with warm (cold) temperature anomalies corresponding to decreases (increases) in sea ice concentration. They report that the Ross Sea SST anomalies are in turn positively correlated with the Nino 3 SST. Their maximum correlation ($r = 0.72$) occurs with a lag of three months with the Ross Sea SST lagging the ENSO signal. Similarly, our results show that south of 50°S, the negative peak in the correlation between the SOI and SST anomalies ($r = -0.7$) is located in the eastern Ross Sea (Fig. 2) with the SST anomalies

lagging the SOI by ~2-3 months. We also found negative (positive) anomalies in ice concentration (Fig. 7), associated with the warmer (cooler) SST and IST.

In an analysis of the length of sea ice season between 1988 and 1994, *Parkinson* [1998] captured one cycle of the SOI. A positive peak in the SOI in 1989 was followed by an ENSO episode in 1992. Based on linear trends over the seven years of data, the results show that the ice seasons have shortened in the eastern Ross Sea, Amundsen Sea, far western Weddell Sea, and non-coastal far eastern Weddell Sea and the coastal regions of East Antarctica, and have lengthened in the western Ross Sea, Bellingshausen Sea and central Weddell Sea., and the 80°E-135°E sector off the coast of East Antarctica. With our results, the difference in the anomalies in the ice extent associated with the SOI^- and SOI^+ extremes (Fig. 7) provide an indication of the trend over the seven years even though the ice extent anomaly is only a proxy indicator of the length of the ice season. We expect the largest variability in length of seasons to be near the ice edge. Over the seven years, our composites indicate that there should be a negative trend in the ice extent over the Ross Sea, the Amundsen Sea, eastern Weddell Sea, and an increase in the Bellingshausen and central Weddell Seas. The anomalies over the East Antarctic sector are not as clear. In general, there is broad agreement with the observed trends especially in the Pacific and Atlantic sectors. Again, these are associated with the co-varying fields of climate and sea ice anomalies linked to the SOI.

In a recent work, *Yuan and Martinson* [2000] summarized the possible relationship between the Antarctic sea ice extent (1978-1996) and global climate variability The also show that the SIE in the Amundsen Sea, Bellingshausen Sea, and Weddell Gyre of the Antarctic polar ocean sectors show the strongest link to extrapolar climate. Our results are in agreement with their observations regarding the relationship between the ENSO signal and the ice extent.

Remarks

Some of the trends and anomalies in the sea ice record discussed above are no doubt associated with the Southern Oscillation. It underscores the importance of placing these

trends and anomalies into a larger context in the interpretation of data sets with a limited temporal record.

5. Conclusions

The spatial signature of the climate and sea ice anomalies in the Southern Ocean associated with the Southern Oscillation are revealed in the correlation patterns and the composite fields. The correlation maps and lag-correlation plots show some features of the spatial and temporal relationships between these anomalies and the index of Southern Oscillation, while the composite maps show the dominant spatial signature of the anomalies during the three phases of SOI. On a large-scale, these anomalies are organized in coherent patterns and assume opposite polarities during the extremes of SOI. Also, these anomalies co-vary with the Southern Oscillation and oscillate at approximately the same frequency. Association with ENSO-related activities in the equatorial Pacific is clearly indicated.

Overall, the anomalies in the Amundsen Sea, Bellingshausen Sea, and Weddell Sea sectors of the Antarctic polar ocean show the strongest link to the Southern Oscillation. Within these sectors, the climate anomalies show the highest correlation with the SOI and the composite patterns show the most extreme and localized climate and sea ice anomalies associated with the extremes of SOI. Positive (negative) phases of the SOI are generally associated with lower (higher) sea-level pressure, cooler (warmer) surface air temperature, and cooler (warmer) sea surface temperature in these sectors. Outside these sectors, the anomalies are not as distinct.

Linkages between the SOI, the climate anomalies, and the sea ice extent, concentration, motion, and ice surface temperature are also evident. The sea ice cover anomalies are located within the same sectors as those with the dominant climate anomalies. During the positive (negative) phase of SOI, positive (negative) anomalies of the SIE are located between 180°W and 130°W in the Ross and Amundsen Seas, negative (positive) anomalies can be found between 100°W and 10°E in Bellingshausen and Weddell Seas,

and, smaller positive (negative) anomalies are found in the sector between 10°E and 50°E.

The physical mechanisms by which these polar processes are linked to the Southern Oscillation are complex and beyond the scope of this study. However, the relationships identified may be useful as diagnostic tools for climate models and for the eventual understanding of the underlying mechanisms of these associations. The composite fields presented can be used as an indicator of the general condition of the Antarctic ice cover during different phase of the Southern Oscillation as measured by the SOI. We have used these fields to explain, in a broad sense, the large-scale trends and anomalies (reported in recent literature) in the sea ice extent and the length of the ice season over the past twenty years. These composite fields are weighted by four strong ENSO episodes over the last 17 years. As a result, the negative trend and negative bias in the SO index have weighted the sea ice and climate anomalies towards the patterns associated with the negative extremes of the SO index.

Data of ice extent and ice area monthly anomalies in the Bellingshausen/Amundsen Sea sector (Fig. 9) show that the ice cover in the region is still declining while those in other regions appear to be increasing slightly. Our analysis shows that spatially, the region is different from other Antarctic regions in that it is influenced by climate parameters in a different way. It is also apparent that the association with SO is strongest in this region. The Antarctic sea ice cover is circumpolar and it is expected that regional trends are small. Our results suggest that the Bellingshausen/Amundsen Seas area is unique partially due to its strong association with the Southern Oscillation.

Acknowledgments

The SMMR and SSM/I brightness temperature and ice concentration fields are provided by World Data Center A for Glaciology/National Snow and Ice Data Center, University of Colorado, Boulder, CO. R. Kwok performed this work at the Jet Propulsion Laboratory, California Institute of Technology under contract with the National Aeronautics and Space Administration.

References

Bendat, J. S. and A. G. Piersol, *Random Data: Analysis and Measurement Procedures*, Third Edition, Wiley-Interscience, 2000.

Bonekamp, H., A. Sterl, and G. J. Komen, Interannual variability in the Southern Ocean from model forced by European Centre for Medium-Range Weather Forecasts reanalysis fluxes, *J. Geophys. Res.*, 104(C6), 13317-13331, 1999

Carleton, A. M., Sea ice-atmosphere signal of the Southern Oscillation in the Weddell Sea, Antarctica, *J. Clim.* 1(4), 379-388, 1988.

Comiso, J. Variability and rends in Antarctic surface temperatures from in-situ and satellite infrared measurements, *J. Clim.*, 13(10), 1674-1696, 2000.

Gloersen, P. Modulation of hemispheric sea-ice cover by ENSO events, *Nature*, 473, 1995.

Jacobs, S.S., and J.C. Comiso, Climate variability in the Amundsen and Bellingshausen Seas, *J. Climate*, 10(4), 697-709, 1997.

Gloersen, P., and A. Mernicky, Oscillatory behavior in Antarctic sea ice concentrations, in Antarctic Research Series, Volume 74, ed. by M. Jeffries, AGU, pp. 161-171, 1998.

Jacobs, S. S. and J. C. Comiso, A Recent Sea-Ice Retreat West of the Antarctic Peninsula, *Geophys. Res. Lett.*, 20(12), 171-1174, 1993.

Kalnay, E. and coauthors, The NCEP/NCAR 40-year reanalysis project, *Bull.Amer. Meteor. Soc.*, 77, 437-471.

Karoly, D. J., Southern Hemisphere circulation features associated with El Nino-Southern Oscillation, *J. Clim.*, 2, 1239-1252, 1989.

King, J. C. and S. A. Harangozo, Climate change in the western Antarctic Peninsula since 1945: observations and possible causes, *Ann Glacol.*, 27: 571-575 1998.

Kwok, R., A. Schweiger, D. A. Rothrock, S. Pang and C. Kottmeier, Sea ice motion from satellite passive microwave imagery assessed with ERS SAR and buoy motions, *J. Geophys. Res.*, 103(C4), 8191-8214, 1998.

Ledley, T. S. and Z. Huang, A possible ENSO signal in the Ross Sea, *Geophys, Res. Lett.*, 24(24), 3253-3256, 1997.

Manabe, S., R. J. Stouffer, M. J. Spelman, and K. Bryan, Transient response of a coupled ocean-atmosphere model to gradual changes of atmospheric CO_2, Part I: Annual mean response, *J Clim.*, 4, 785-818, 1991.

Mo, K. C. and G. H. White, Teleconnections in the Southern Hemisphere, *Mon. Wea. Rev.*, 113, 22-37, 1985.

Parkinson, C.L., Length of the sea ice season in the southern ocean, in Antarctic Research Series, Volume 74, ed. by M. Jeffries, AGU, pp. 173-186, 1998.

Peterson. R. G. and W. B. White, Slow oceanic teleconnections linking the Antarctic Circumpolar Wave and the tropical El Nino-Southern Oscillation, *J. Geophys. Res.*, 103(C11), 24573-24583, 1998.

Philander, S. G. and E. M. Rasmussen, The Southern Oscillation and El Nino, Advances in Geophys., 28A, 197-215, 1985.

Reynolds, R. W. and T. M. Smith, Improved global sea surface temperature analyses using optimal interpolation, *J. Clim.*, 7, 929-948, 1994.

Schlesinger, M. and J. Mitchell, Model projections of the equilibrium climatic response to increased carbon dioxide, *in The Potential Climatic Effects of Increasing Carbon Dioxide*, DOE/ER-0237, 81-148, US Dept of Energy, 1985.

Simmonds, I. and T. H. Jacka, Relationships between the Interannual Variability of Antarctic Sea Ice and the Southern Oscillation, *J. Clim.*, 8, 637-647, 1995.

White, W. B. and R.G. Peterson, An Antarctic circumpolar wave in surface pressure, wind, temperature and sea ice extent, *Nature*, 380, 699-702, 1996.

Yuan, X. and D. G. Martinson, Antarctic sea ice extent variability and its global connectivity, *J. Clim.*, 13, 1797-1717, 2000.

Figure Captions

Figure 1. The Southern Oscillation Index between 1978 and 1999 and its wave-number spectrum between 1982 and 1998.

Figure 2. Correlation of climate anomalies with SOI time series (1982-1998) and location of the positive (black) and negative (white) extremes on the correlation maps. The correlation coefficients are statistically significant at the 95% level if they exceed a threshold of ~0.25 (see text).

Figure 3. Lag-correlation plots of the SLP, SAT, and SST anomalies with the SOI time series at the positive and negative correlation extremes. (positive indicates SOI leads). The autocorrelation of the SOI time series is also shown.

Figure 4. Composites of climate anomalies (1982-1998) during three phases of SOI (SOI > 0, 0 > SOI > -1, SOI < -1) and the difference between the two extremes (SOI > 0 and SOI < -1).

Figure 5. Composites of winter ice motion anomalies (March-Nov, 1982-1998) during three phases of SOI (SOI > 0, 0 > SOI > -1, SOI < -1) and the difference between the two extremes (SOI > 0 and SOI < -1).

Figure 6. Composites of ice surface temperature anomalies (January and July, 1982-1998) during three phases of SOI (SOI > 0, 0 > SOI > -1, SOI < -1) and the difference between the two extremes (SOI > 0 and SOI < -1).

Figure. 7. Composites of ice edge/concentration anomalies (1982-1998) during three phases of SOI (SOI > 0, 0 > SOI > -1, and SOI < -1) and the difference between the two extremes (SOI > 0 and SOI < -1).

Figure. 8. Lag-correlations between sea ice edge anomalies and SOI (1982-1998). (positive indicates that SOI leads).

Figure. 9. Anomalies in sea ice extent, area, and concentration in the Amundsen/Bellingshausen Seas from 1978-1999.

Sea Ice Processes/Southern Ocean
Southern Oscillation Index (78-99) (SOI)

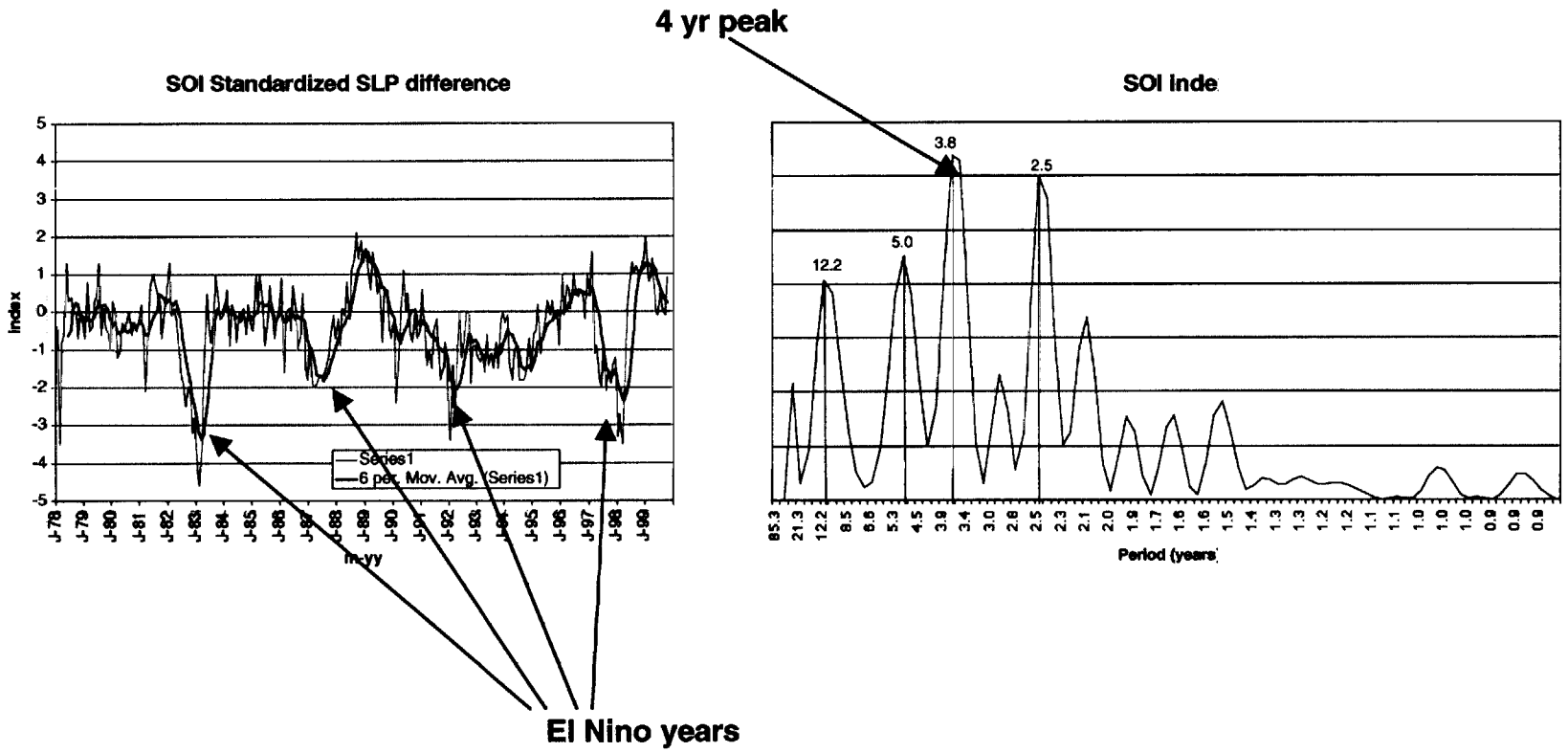

SOI - difference between the standardized Tahiti SLP and standardized Darwin SLP
Extreme negative SOI indices are associated with ENSO.

1/26/01

Fig. 1 RK/JCC

Sea Ice Processes/Southern Ocean

Correlation of Climate Anomalies with SOI

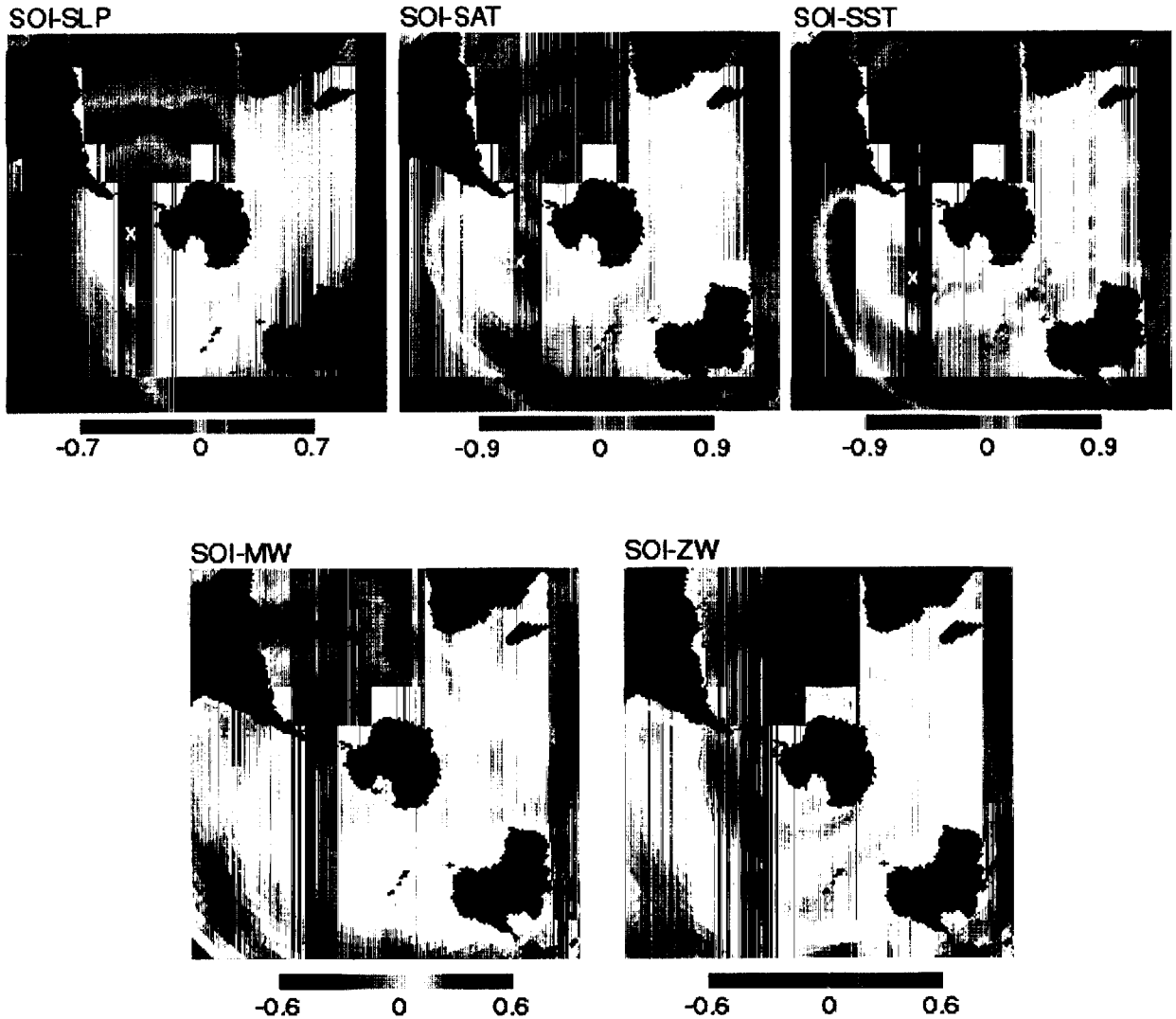

1/26/01

Fig. 2 RK/JCC

Sea Ice Processes/Southern Ocean

Lag-Correlation of Climate Anomalies w/SOI

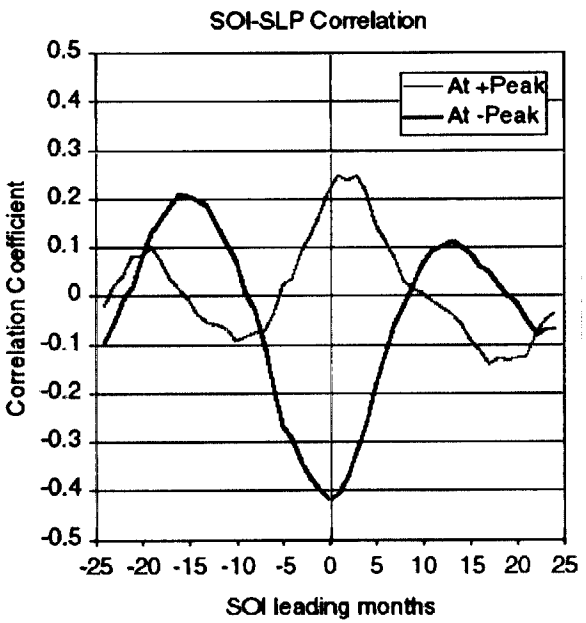

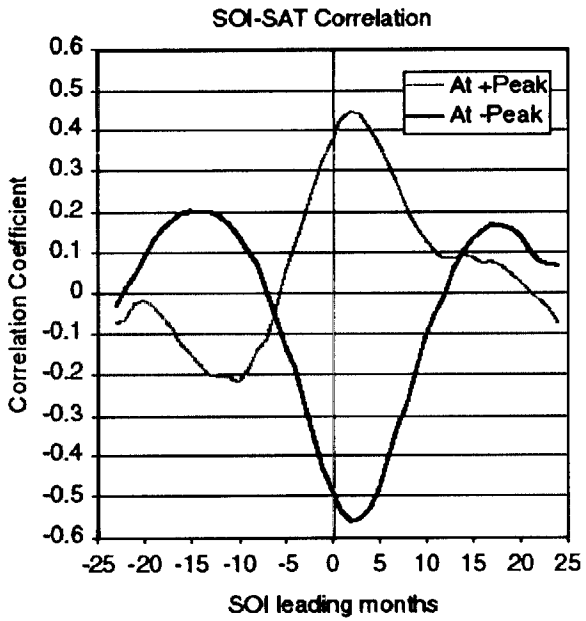

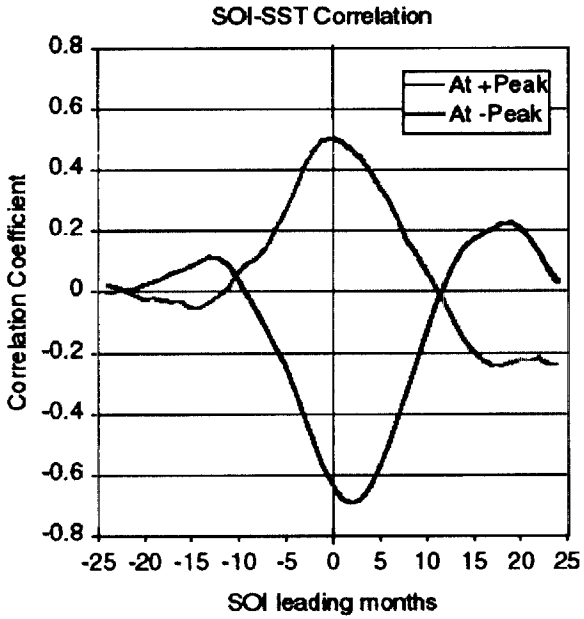

1/26/01

Fig. 3 RK/JCC

Sea Ice Processes/Southern Ocean
Climate Anomalies (3 phases of SOI)

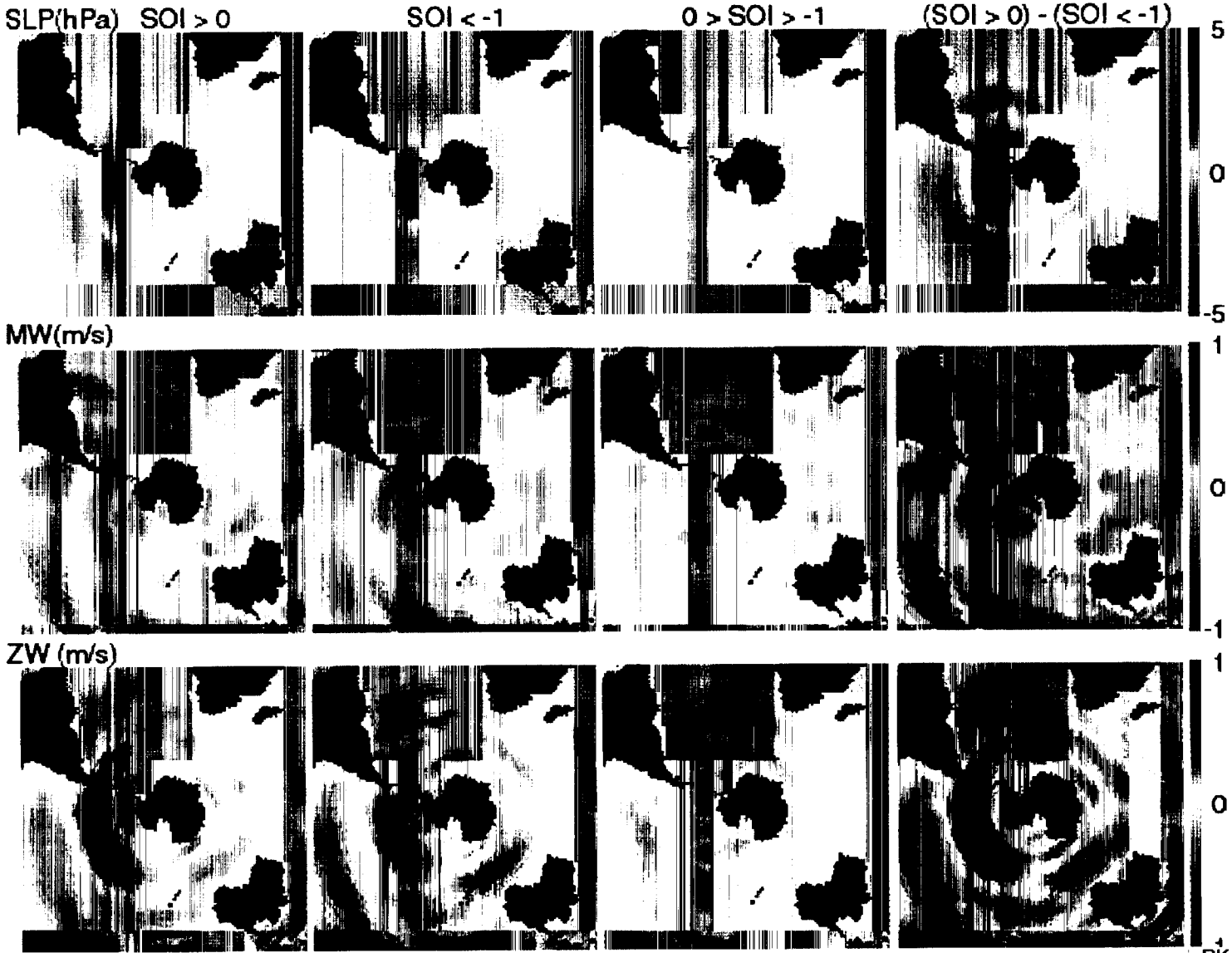

1/26/01

RK/JCC

Fig. 4a

Sea Ice Processes/Southern Ocean
Climate Anomalies (3 phases of SOI)

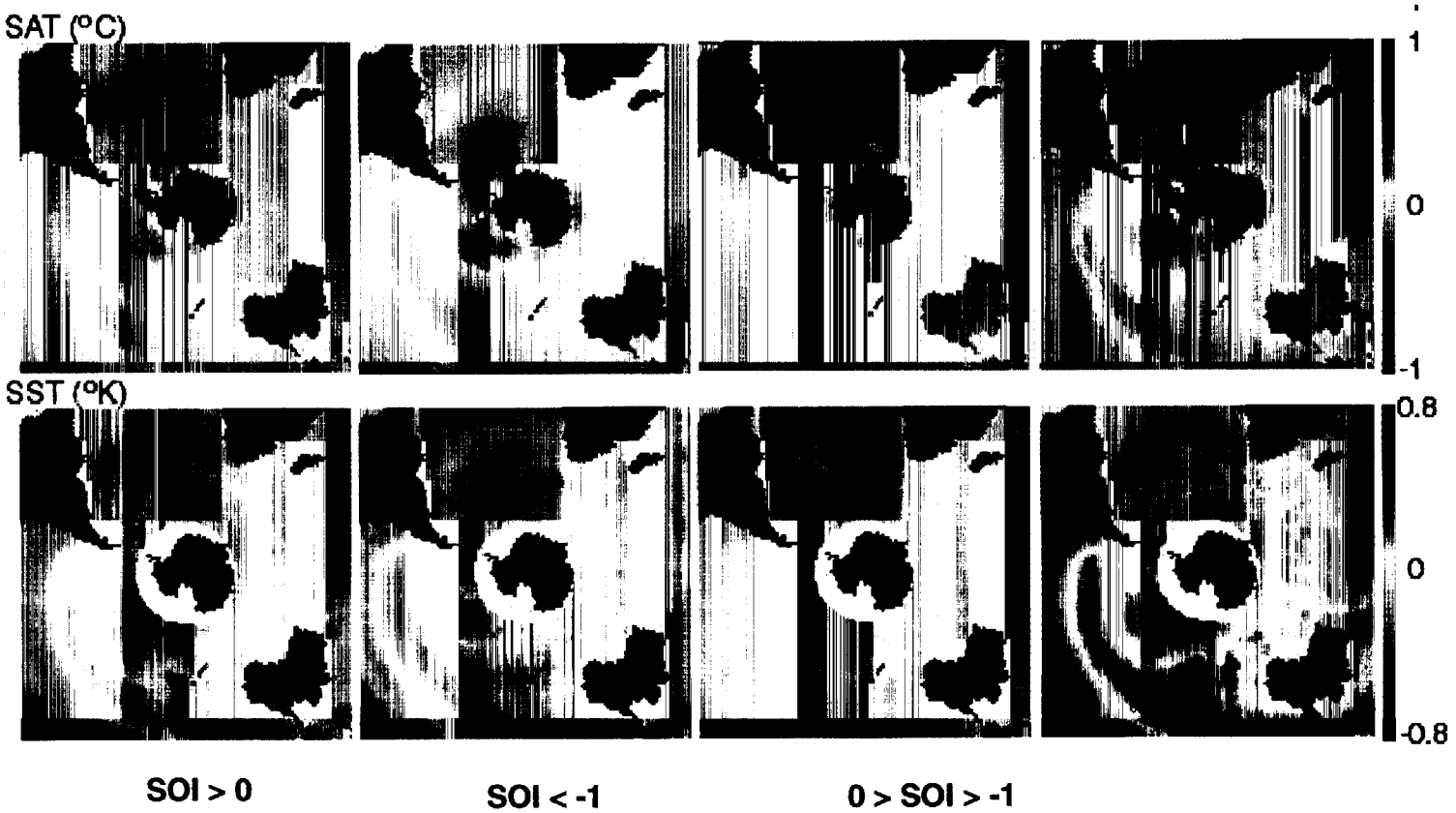

Sea Ice Processes/Southern Ocean
Ice Motion Anomalies

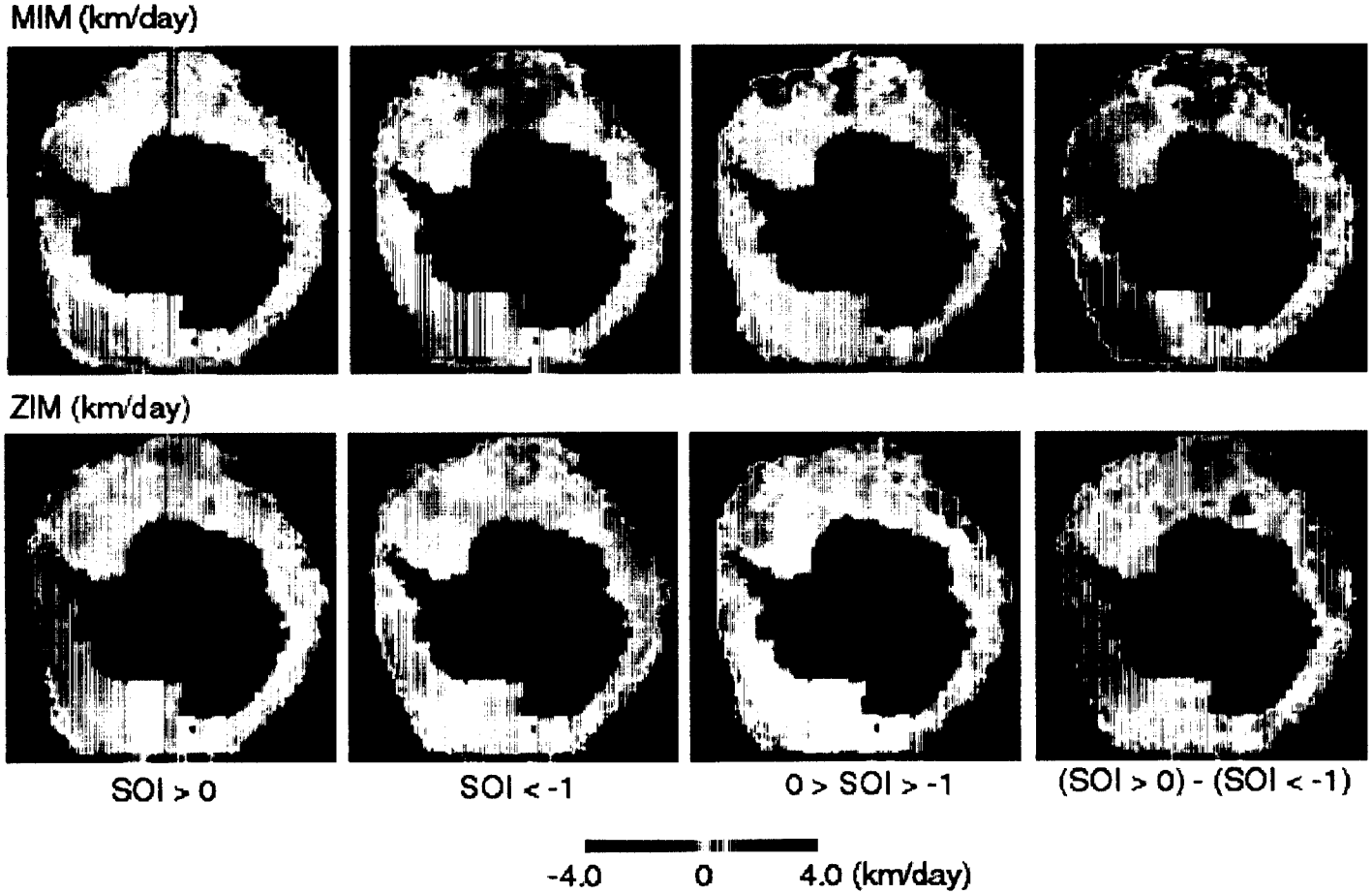

1/26/01

Fig. 5 RK/JCC

Sea Ice Processes/Southern Ocean
Ice Surface Temperature Anomalies

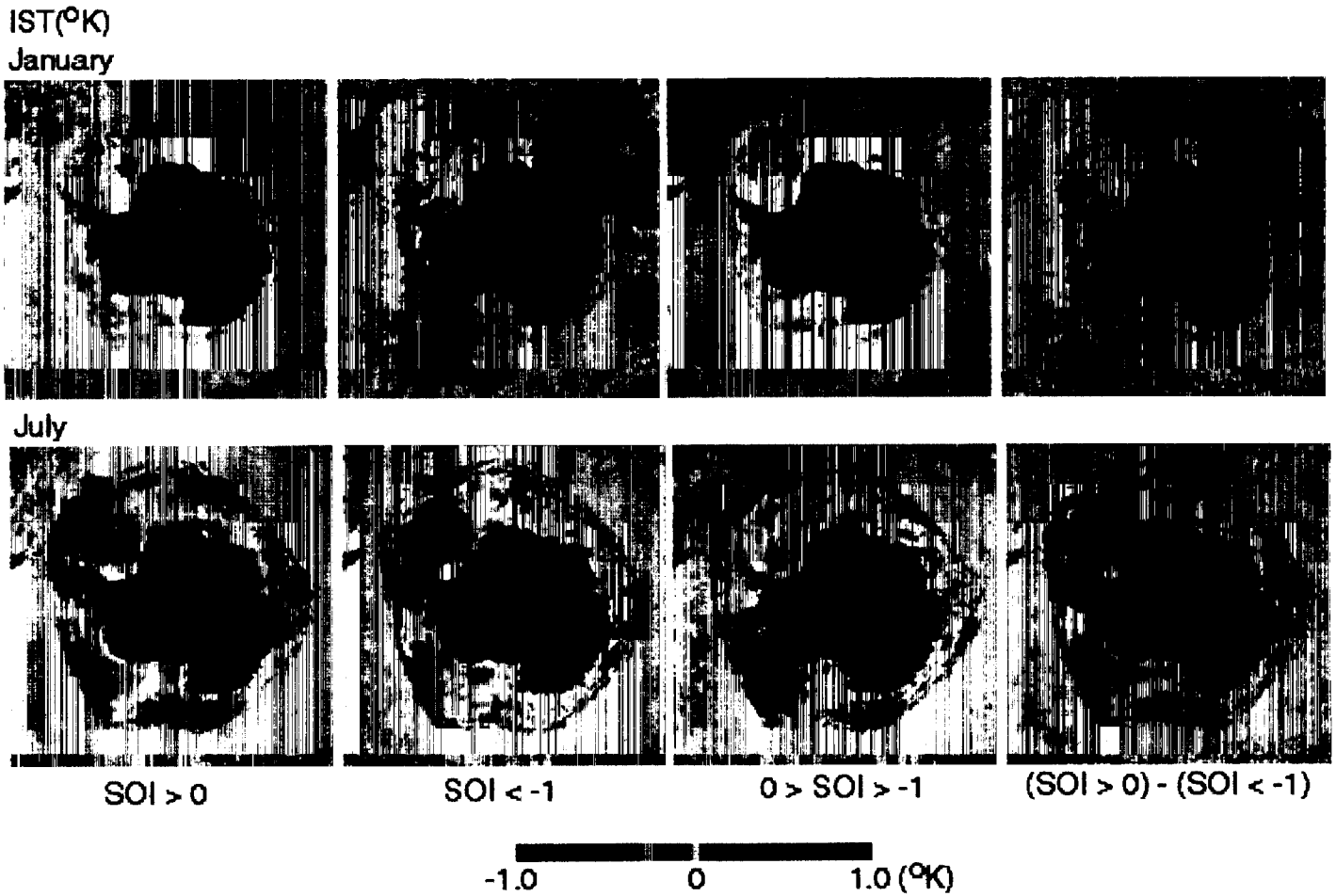

1/26/01

Fig. 6 RK/JCC

Sea Ice Processes/Southern Ocean
Ice Edge/Ice Concentration Anomalies

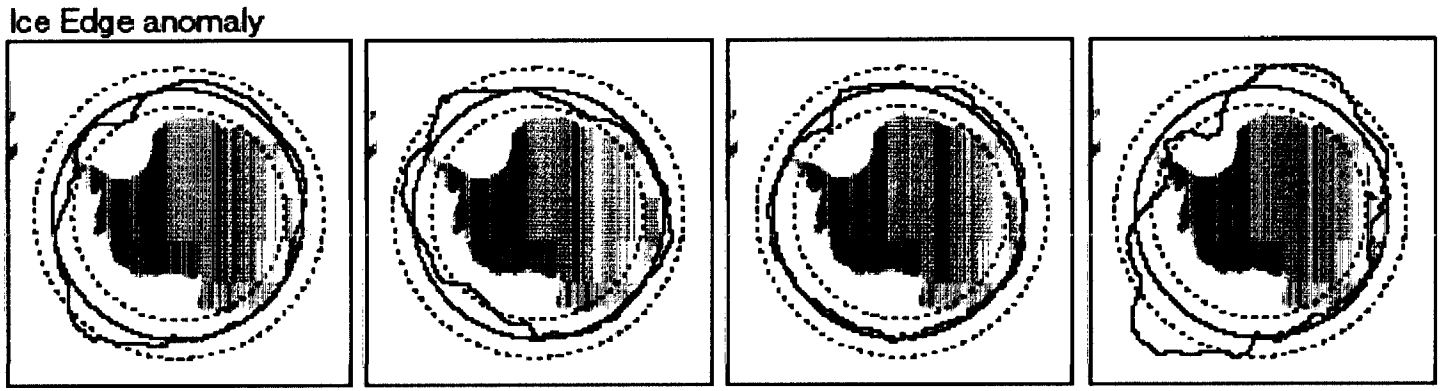

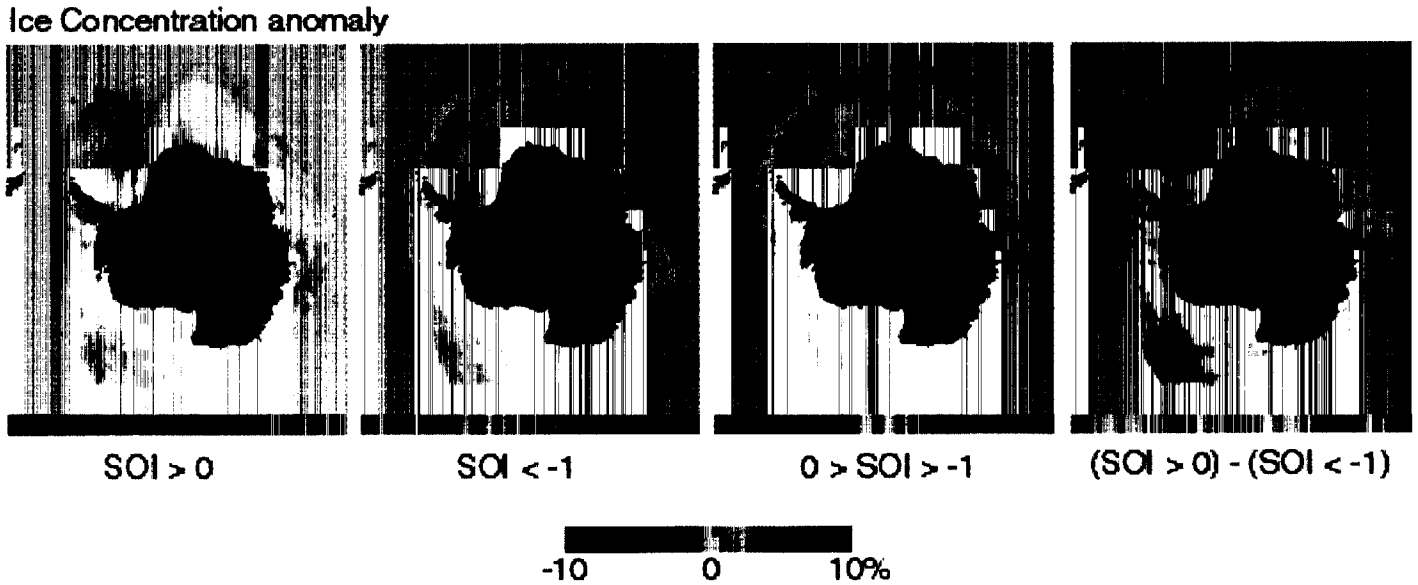

1/26/01

Fig. 7 RK/JCC

Sea Ice Processes/Southern Ocean
Lag Correlation SOI vs Ice edge

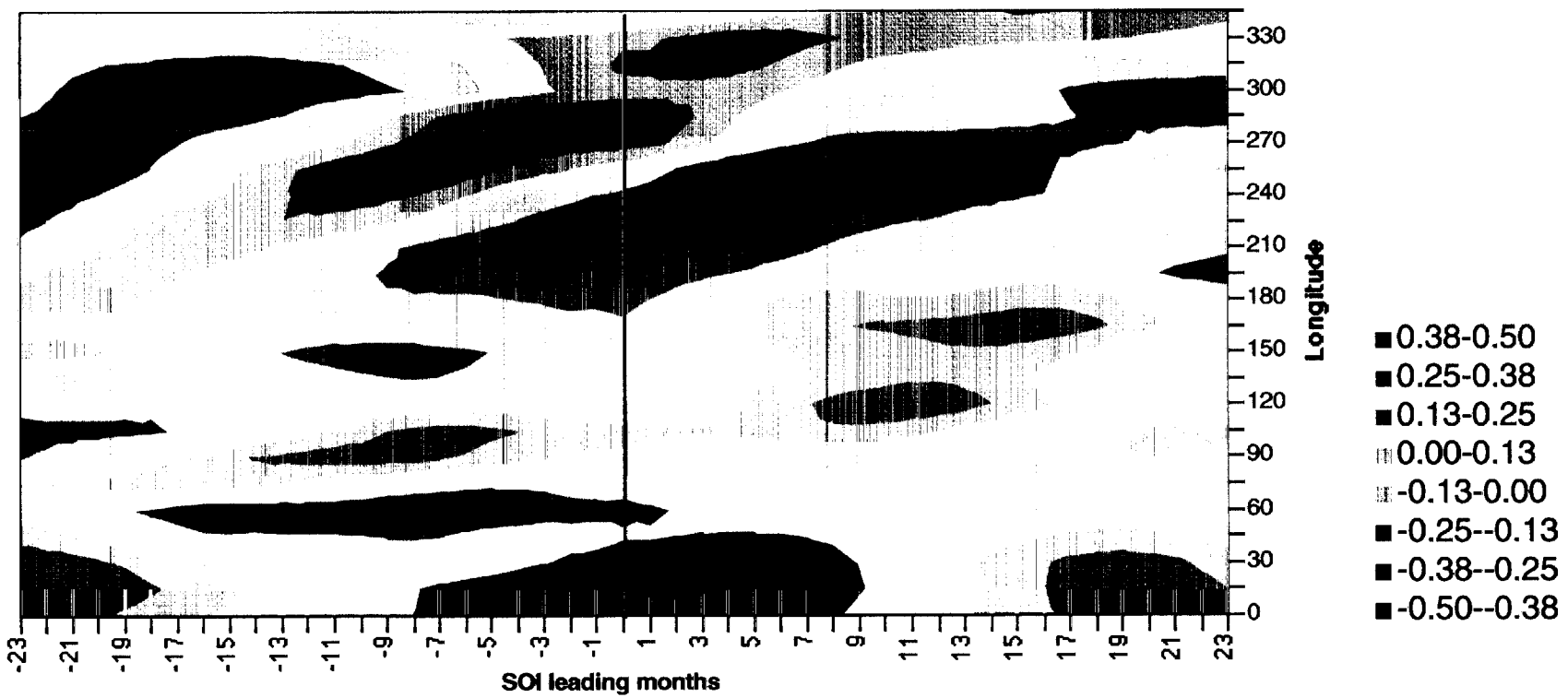

1/26/01

Fig. 8 RK/JCC

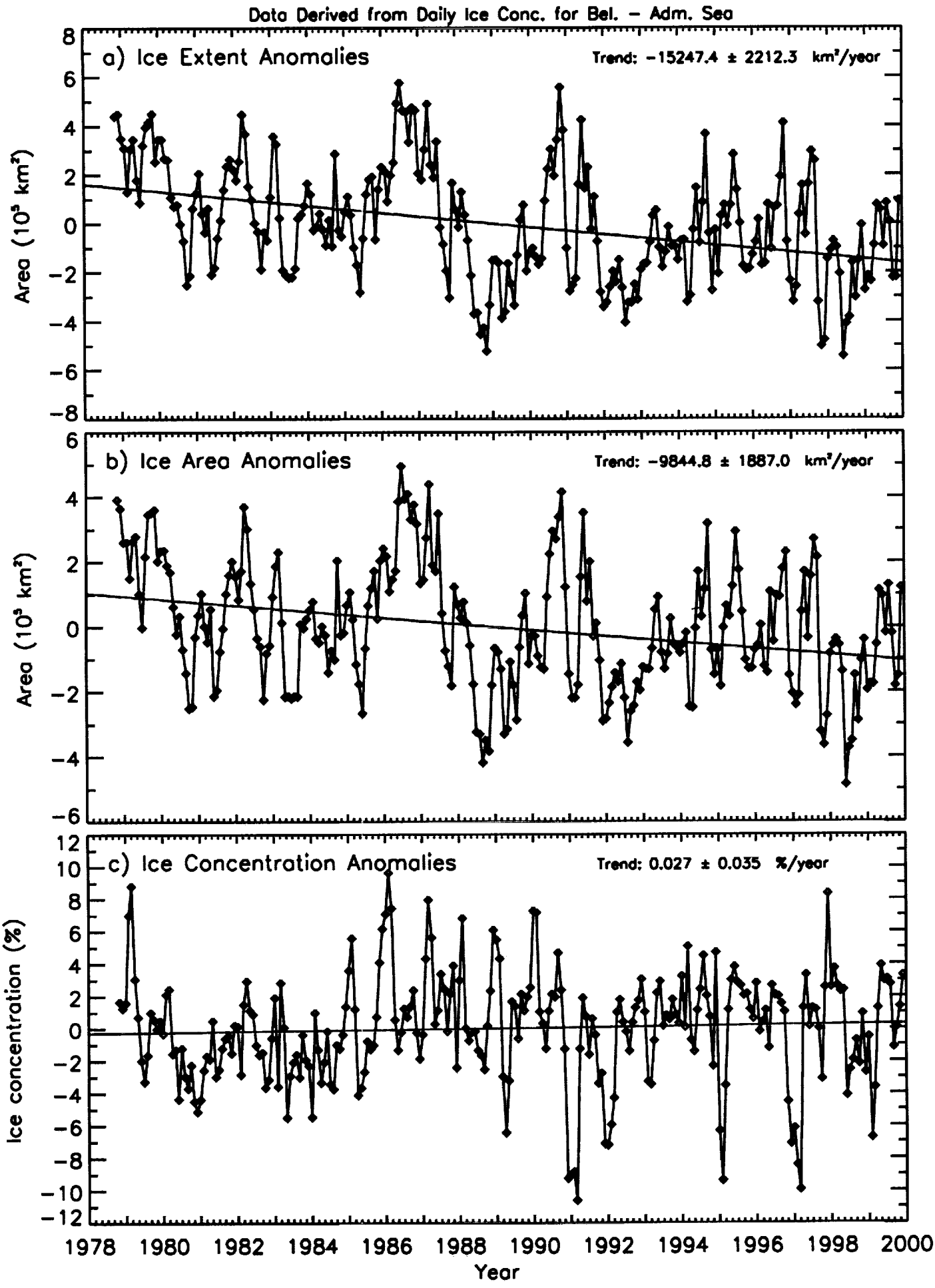
Data Derived from Daily Ice Conc. for Bel. – Adm. Sea
a) Ice Extent Anomalies
Trend: −15247.4 ± 2212.3 km²/year
Area (10³ km²)
b) Ice Area Anomalies
Trend: −9844.8 ± 1887.0 km²/year
Area (10³ km²)
c) Ice Concentration Anomalies
Trend: 0.027 ± 0.035 %/year
Ice concentration (%)
1978 1980 1982 1984 1986 1988 1990 1992 1994 1996 1998 2000
Year

Fig. 9